Highly efficient organic light-emitting diodes from delayed fluorescence

Uoyama, Hiroki
Center for Organic Photonics and Electronics Research, Kyushu University

Goushi, Kenichi
International Institute for Carbon Neutral Energy Research (WPI-I2CNER), Kyushu University | Center for Organic Photonics and Electronics Research, Kyushu University

Shizu, Katsuyuki
Center for Organic Photonics and Electronics Research, Kyushu University

Nomura, Hiroko
Center for Organic Photonics and Electronics Research, Kyushu University

他

出版情報：Nature. 492 (7428), pp.234-238, 2012-12-12. Nature Publishing Group
バージョン：

Third Generation Organic LED by Hyper-Fluorescence

Hiroki Uoyama, Kenichi Goushi, Katsuyuki Shizu, Hiroko Nomura, and

Chihaya Adachi

Center for Organic Photonics and Electronics Research (OPERA), Kyushu University

744 Motooka, Nishi, Fukuoka 819-0395, Japan

Although typical organic molecules are simply composed of carbon (C), hydrogen (H), nitrogen (N) and oxygen (O) atoms, carbon's unique bonding manners based on sp^3, sp^2 and sp hybrid orbitals enable very complicated molecular architectures, leading to amazing functions in a wide variety of creatures and industrial products. In the last two decades, the allure of unlimited freedom of design with organic molecules has shifted a significant part of the research effort on electronics from inorganic into organic materials. In particular, great progress has been achieved in the development of organic light-emitting diodes (OLEDs). The successive progress of 1st generation OLEDs using fluorescent molecules and 2nd generation OLEDs using phosphorescent molecules solidified organic materials as a very attractive system for practical electronics. In this study, we designed new advanced electroluminescent (EL) molecules composed of only conventional CHN atoms without any precious metals. With proper molecular design, the energy gap between the two excited states, *i.e.*, singlet (S_1) and triplet (T_1) excited states, are minimized, promoting very efficient spin up-conversion from T_1 to S_1 states (reverse intersystem crossing (ISC)) while maintaining a rather high radiative decay rate of $>10^6$/s, leading to a high fluorescence efficiency of >90%. Using these unique molecules, we realized a very

high external EL efficiency of over 19% that is comparable with those of high-efficiency phosphorescence-based OLEDs. Thus, these molecules harvest both singlet and triplet excitons for light emission under electrical excitation through fluorescence decay channels. We call this new luminescence concept "Hyper-fluorescence".

The recombination of holes and electrons can produce light that is referred as electroluminescence (EL). EL in organic materials was first discovered by M. Pope et al. in 1963 using an anthracene single crystal connected to high-field carrier injection electrodes[1]. Carriers of both signs were injected into the organic layers, and the subsequent carrier transport and recombination produced blue EL that originates from singlet excitons, *i.e.*, fluorescence. In principle, carrier recombination is expected, according to spin statistics, to produce both singlet and triplet excitons in the ratio of 1:3[2,3], and this relationship has been well demonstrated for many cases[4,5]. The produced singlet excitons decay promptly, yielding prompt EL (fluorescence), while two triplet excitons can fuse to form a singlet exciton through triplet-triplet annihilation, yielding delayed EL (delayed fluorescence). On the other hand, while the direct radiative decay of triplet excitons results in phosphorescence, it usually occurs only at very low temperatures in conventional organic aromatic compounds. In fact, in 1990, one of

authors, C. A., reported the first demonstration of phosphorescent EL using keto-coumarin derivatives[6]. However, the very faint EL was observed at 77 K with difficulty and was assumed to be virtually useless in most cases, even if including rare earth complexes[7]. In 1999, Forrest and Thompson's group first demonstrated efficient electrophosphorescence using iridium phenylpyridine complexes that promote an efficient radiative decay rate of ~10^6/s by taking advantage of a heavy metal effect, strong spin-orbital coupling[8]. Nearly 100% internal EL efficiency was demonstrated[9], providing convincing evidence that OLED technology could be useful for display and lighting applications.

In this report, we achieved a novel pathway to reach the ultimate EL efficiency by inventing simple aromatic compounds displaying efficient thermally-activated delayed fluorescence (TADF) with high photoluminescence (PL) efficiency. **Figure 1 (a)** shows the energy diagram of a conventional organic molecule, depicting singlet (S_1) and triplet (T_1) excited states with a ground state (S_0). While we had previously assumed that the S_1 level should be significantly higher than the T_1 level, *i.e.*, 0.5~1.0 eV higher, due to the presence of electron exchange energy, we found that the proper design of organic molecules can lead to a small energy gap (ΔE_{ST}) between them[10,11]. Relatedly, a molecule displaying efficient TADF requires a very small ΔE_{ST} between its S_1 and T_1

excited states, resulting in enhanced $T_1 \rightarrow S_1$ reverse intersystem crossing (ISC). Such excited states are attainable by the intramolecular charge transfer (CT) of a spatially separated donor and acceptor system.[11] The critical point of the molecular design is the compatibility of a small $\Delta E_{ST} \sim 0$ eV and a reasonable radiative decay rate of over 10^6/s that overcomes competitive non-radiative decay paths, leading to highly luminescent TADF materials. Since the two properties conflict with each other, a delicate balance of the overlap of the highest occupied molecular orbital (HOMO) and lowest unoccupied molecular orbital (LUMO) is required. Furthermore, to enhance the PL efficiency of a TADF material, geometrical change between its S_0 and S_1 states should be restrained to suppress non-radiative decay processes. Since very small orbital overlapping generally results in virtually no emission as is shown in benzophenone derivatives, one assumes that high PL efficiency could never be obtained with molecules having small ΔE_{ST}; however, we have overcome this issue.

In this work, we designed a novel series of highly efficient TADF emitters, which are based on carbazolyl dicyanobenzene (CDCB) having carbazole as a donor and dicyanobenzene as an electron acceptor as shown in **Fig. 1 (b)**. Since the steric carbazolyl unit is significantly distorted against the dicyanobenzene plane by their steric hindrance to each other, the HOMO and LUMO can be localized around the donor and

the acceptor moieties, respectively, leading to a small $\Delta E_{ST.}$ Moreover, the dicyanobenzene and carbazolyl groups play important roles in obtaining high PL efficiency and various emission colors, respectively. Dicyanobenzene derivatives are known to alter their chemical bonds upon changing their electronic properties in excited states[12]. We expect the following advantages from CDCBs based on the density functional theory (DFT) calculations as described below. The change in the geometry of CDCBs between S_0 and S_1 states occurs not all over the molecule but only in the central dicyanobenzene unit, and the inhibition of large geometry change leads to a high quantum efficiency. On the other hand, the emission wavelength of CDCBs can be readily tuned by changing the electron donating ability of the peripheral groups, which can be altered by the number of carbazolyl groups or the introduced substituents. On the basis of molecular design, CDCBs allow us to achieve not only highly efficient TADF but also a wide palette of emission colors.

CDCBs were synthesized through a one-step-only reaction from commercially available starting materials without the addition of palladium or other rare metal catalysts, indicating that CDCBs also have cost advantages. The aromatic nucleophilic substitution reaction (S_NAr) of an anion of carbazole, generated by treatment with NaH and dicyanobenzene at room temperature, yielded CDCBs. All CDCBs except 4CzPN

and 2CzPN were obtained with high yields over 79%, while 4CzPN and 2CzPN were obtained with lower yields (38 and 9%, respectively) due to purification problems. Full characterization of CDCBs was performed by NMR, IR, HR-MS and elemental analysis (see Supplementary Information). CDCBs showed high thermal stability; for example, the sublimation of 4CzIPN started around 450 °C before decomposition in thermogravimetric analysis (TGA) under nitrogen-flow conditions.

Figure 2 (a) indicates UV-vis absorption and PL spectra of 4CzIPN in toluene with a concentration of 10^{-5} mol/l. 4CzIPN shows an intense green-emission with a maximum at a wavelength of 507 nm and high PL quantum yield (PLQY) (Φ = 94±2%). The Stokes shift is very small; generally, the emission produced by intramolecular charge transfer between a donor and an accepter unit shows a large Stokes shift.[13] Under a nitrogen-saturated condition, the delayed component of $\tau \sim 5.1 \pm 0.5$ μs is more than two orders longer than the prompt component of $\tau \sim 17.8 \pm 1$ ns (see Supplementary Information). To investigate whether the triplet state is involved in luminescence, the transient PL and the PLQY of 4CzIPN were measured in toluene under oxygen atmosphere. When the solution of 4CzIPN in toluene was bubbled with oxygen for 10 min, the lifetime of the delayed component became very short at $\tau \sim 91 \pm 3$ ns with a prompt component of $\tau \sim 6.9 \pm 0.5$ ns, and the PLQY decreased to 10%. These results

apparently suggest that 4CzIPN is a TADF material, since the delayed fluorescence was significantly quenched by oxygen[11].

We optimized the geometry of the S_0 state of 4CzIPN with the PBE0 functional[14] and the 6-31G(d) basis set[15] employing density-function-theory (DFT). Geometry optimizations of the S_1 and T_1 states were carried out at the same level with the time-dependent DFT (TD-DFT) procedure. All of the *ab initio* calculations were done assuming C_2 symmetry using the Gaussian 09 software.[16] **Figures 2 (b) and (c)** show the HOMO and LUMO distributions of 4CzIPN, respectively, for the optimized structure of the S_0 state. The S_1 and T_1 states correspond to a HOMO-LUMO transition and display a CT character. The HOMO is delocalized over the four carbazolyl moieties, while the LUMO is distributed on the dicyanobenzene moiety; the carbazolyl groups act as electron donors, while the dicyanobenzene acts as an electron acceptor. Steric hindrance between the carbazole and dicyanobenzene moieties causes large dihedral angles of about 60° between the carbazole and dicyanobenzene planes. Consequently, the HOMO and LUMO are spatially well-separated, and the exchange interaction between the electrons in the HOMO and LUMO is weak, leading to a small S_1-T_1 energy splitting and enhancement of $T_1 \rightarrow S_1$ reverse ISC.

As stated above, the Stokes shift of the S_1 state of 4CzIPN is rather small

compared with those from typical charge transfer states, suggesting small geometry relaxation due to $S_1 \leftarrow S_0$ excitation. In general, bond-length change originating from an electronic excitation is large where the electron-density difference $\Delta\rho$ due to the excitation is largely distributed. **Figure 2 (d)** shows $\Delta\rho$ resulting from the $S_1 \leftarrow S_0$ excitation of 4CzIPN. $\Delta\rho$ is largely distributed on the dicyanobenzene moiety (electron acceptor), especially on the C_3-C_4 and C_6-C_1 bonds. The remaining $\Delta\rho$ spreads over the carbazolyl moieties (electron donors). In order to investigate the geometry change quantitatively, we calculated the differences between the S_1 and S_0 state bond lengths of 4CzIPN. The geometry change was found to occur mainly in the dicyanobenzene moiety, reflecting the large $\Delta\rho$ distribution on it. Thus, the strong electron-accepting ability of dicyanobenzene is responsible for the small geometry relaxation.

Figure 2 (e) shows the differences between the S_1 and S_0 state bond lengths in the dicyanobenzene moiety of 4CzIPN. The bond-length changes are large in the C_3-C_4 and C_6-C_1 bonds, while they are small in the C_7-N_1 and C_8-N_2 triple bonds, suggesting that a quinoid-type geometry relaxation does not occur in the S_1 state of 4CzIPN. The lack of the quinoid-type deformation accounts for the small geometry relaxation of 4CzIPN compared with those of 4CzTPN and 4CzPN. Consequently, 4CzIPN exhibits a smaller Stokes shift and higher PLQY than those of 4CzTPN and 4CzPN. On the carbazolyl

moieties, since $\Delta\rho$ is quite small, the geometry change is also small. In fact, the calculated bond-length changes in the C-C and C-N bonds on the carbazolyl moieties are at most 0.0015 Å. In addition, we note that while the oscillator strength for the ground states of CDCBs estimated by TD-DFT is a rather small value of less than 0.1, the peculiar geometric characteristics discussed in this paragraph are consistent with the suppression of the non-radiative decay, leading to the high PLQY.

Figure 3 shows the PL spectra of CDCBs in toluene. The series of CDCBs achieved a wide palette of emission colors ranging from sky-blue (473 nm) to orange (577 nm). The emission wavelength is dependent on the electron-donating and the electron-accepting ability of the peripheral carbazolyl groups and the central dicyanobenzene unit, respectively. Introduction of methyl or phenyl to the 3- and 6-positions of the carbazolyl groups of 4CzTPN provides a red shift of the emission maximum from 535 to 561, 553, and 577 nm, respectively. On the other hand, in the case of 2CzPN, the presence of less carbazolyl groups damps the electron-donating ability and produces a blue shift of the emission maximum. PLQY and transient PL of CDCBs were measured in toluene under a nitrogen atmosphere, as summarized in Supplementary Information. 4CzPN and 4CzTPN show high PLQY (Φ = 74±3 and 72±3%, respectively), while 4CzTPN-Me, 4CzTPN-Ph and 2CzPN provide lower

PLQYs (Φ = 47±2, 26±1 and 47±2%, respectively) due to the presence of substituents or less carbazolyl groups. Since the transient PL of all CDCBs showed both a nanosecond-scale prompt component and a microsecond-scale delayed component, the series of CDCBs were confirmed to be TADF materials.

Figure 4 (a) shows the PL decay curves for 4CzIPN emission at 100, 200, and 300 K in a 6wt%-4CzIPN: 4,4'-bis(carbazol-9-yl)biphenyl (CBP) film. The triplet excitons of 4CzIPN are well confined using a CBP host since the triplet excited state of CBP is higher than the singlet excited state of 4CzIPN. In addition, CBP fluorescence is completely quenched due to the efficient energy transfer between the guest and host molecules. The intense emissions around t=0 s correspond to the prompt component, and the long tail emissions correspond to the delayed fluorescence component. The prompt component is assigned to the fluorescence, while the delayed component can be assigned to the delayed fluorescence via the reverse ISC process, *i.e.*, TADF, since the PL spectrum of the delayed fluorescence is identical to that of the prompt fluorescence, as shown in **Fig. 4 (b)**. **Figure 4 (c)** shows the temperature-dependent PLQYs for the prompt and delayed components of the film. The two components are resolved by combining the absolute PLQY estimated by an integrated sphere photoluminescence measurement system and the temperature dependence of the PL decay curves

(**Supplementary Information**). The prompt component very slightly increases with a decrease in temperature, indicating the suppression of non-radiative decay from the singlet state. On the other hand, the delayed component monotonically decreases with a decrease in temperature, since the reverse ISC process becomes the rate-determining step, similar to the temperature dependence of tin(IV) fluoride-porphyrin complexes, which are typical TADF emitters[10]. At room temperature of 300 K, a high PLQY of 83±2% was observed. To quantitatively evaluate ΔE_{ST}, the activation energy of the reverse ISC rate constant (k_{RISC}) was estimated based on $\exp(-\Delta E_{ST}/k_B T)$, where k_B is Boltzmann's constant and T is the temperature. k_{RISC} can be estimated from the experimentally observable rate constants and the PLQYs of the prompt and delayed components using the following equation[17]

$$k_{RISC} = \frac{k_p k_d}{k_{ISC}} \frac{\Phi_d}{\Phi_p} \qquad (1)$$

where k_p and k_d are the rate constants of the prompt and delayed fluorescence components, respectively, k_{ISC} is the ISC rate constant from singlet to triplet states, and Φ_p and Φ_d are the PLQYs of the prompt and delayed components, respectively. k_{RISC} is estimated using **Eq. 1**, and is shown in **Fig. 4 (d)** as a function of $1/T$ (Arrhenius plot) between 200 and 300 K, assuming that k_{ISC} is independent of temperature. An activation energy of 83 meV was estimated. Therefore, the k_{RISC} would be significantly suppressed

at low temperature. However, even at low temperature, the PLQY of the delayed component is still high at over 40%, implying that the reverse ISC rate constant is relatively higher than the non-radiative rate constant of the triplet state. It should be noted that below 200 K, the decay curves do not agree with the double exponential decay model, but well correspond to a multi-exponential decay model. This can be explained by the widened ΔE_{ST} distribution caused by inhomogeneous molecular environments.

We evaluated OLED performance using CDCB as an emitter. To demonstrate the OLED characteristics and the color variation of CDCB derivatives, we selected 4CzIPN (green emission), 4CzTPN-Ph (orange emission), and 2CzPN (sky-blue emission). **Figure 5** shows the external EL quantum efficiency of OLEDs based on CDCB derivatives showing from sky-blue to orange emission. To achieve high EL efficiency in OLEDs using CDCB derivatives, the triplet excited state of the CDCB derivatives must be confined using host materials with higher triplet energy levels. Therefore, we used CBP as a host material in the green and orange OLEDs and 2,8-bis(diphenylphosphoryl)dibenzo[*b*,*d*]thiophene (PPT) as a host material in the sky-blue OLED. The device structures consist of ITO / α-NPD (35nm) / 2wt% 4CzIPN or 6wt% 4CzTPN-Ph:CBP (15nm) / TPBi (65nm) / LiF / Al and ITO / α-NPD (40nm) /

mCP (10nm) / 6wt% 2CzPN:PPT (20nm) / PPT (40nm) / LiF / Al. In the green OLED, we achieved the very high external EL quantum efficiency of 19.3±1.5% which would be equivalent to an internal EL quantum efficiency of ~100%, assuming a light out-coupling efficiency of 20%. In addition, the orange and sky-blue OLEDs show higher external EL quantum efficiency of 11.2±1% and 8.0±1%, respectively, compared to those of conventional fluorescence-based OLEDs.

Finally, we discuss the driving force for the efficient reverse ISC without heavy metals. It is generally accepted that the introduction of the spin-orbit coupling that is provided by heavy atoms is indispensable for both efficient ISC and reverse ISC. Thus, metal complexes having heavy metals and aromatic compounds having halogens and carbonyls can promote efficient spin conversion. On the other hand, our molecular design contains no such kind of atoms, while very efficient spin conversion was realized. This is because the first-order mixing coefficient between singlet and triplet states (λ) is inversely proportional to the ΔE_{ST} as described by[18]:

$$\lambda = \frac{H_{SO}}{\Delta E_{ST}} \qquad (2)$$

where H_{SO} is the spin-orbital interaction. Thus, we do not necessarily have to include heavy atoms for efficient spin conversion once we realize small ΔE_{ST}, which opens more freedom for the molecular design of TADF materials.

In summary, it was believed that high PLQY was incompatible with small ΔE_{ST} due to the separation of HOMO from LUMO, since the separation usually leads to small radiative decay rates. However, CDCBs realized a breakthrough on this front. Therefore, the synthesized materials are classified as unprecedented novel EL materials that realize ultimate EL efficiency, which we name “Extreme-fluorescence”. Although the use of phosphorescence such as iridium phenylpyridine derivatives has been assumed to be a sole solution to obtain ultimate EL efficiency, our results clearly open a novel way for high efficiency just by combining very common aromatic parts. Our demonstration convincingly shows that finely tuned molecular design can provide unexpected functions and reminds us of the great flexibility of organic molecules. We hope that our novel molecules will contribute to upcoming solid-state lighting and display applications.

Methods

Synthesis of carbazolyl dicyanobenzene

General experimental details, synthesis and characterization for all compounds can be found in the Supplementary Information. CDCBs were synthesized by reaction of a carbazolyl anion and a fluorinated dicyanobenzene at room temperature for 10 h under a nitrogen atmosphere. Purification of CDCBs was performed by silica-gel chromatography and/or reprecipitation. Moreover, CDCBs for PL and EL measurements were purified by sublimation.

PL measurements

Organic films for optical measurements were fabricated by thermal evaporation under a high vacuum (ca. 7×10^{-4} Pa) onto clean quartz and silicon substrates. The PL spectra of these films were recorded with a spectrofluorometer (Horiba Jobin Yvon, FluoroMax-4), and the PL quantum efficiencies were measured using an absolute PL quantum yield measurement system (Hamamatsu, C9920-02). The transient PL characteristics were measured under vacuum using a streak camera (Hamamatsu, C4334). A nitrogen-gas laser with a wavelength of 337 nm and a pulse width of approximately 500 ps (Lasertechnik Berlin, MNL200) was used as an excitation source.

Low temperature measurements were conducted using a cryostat (Iwatani Industrial Gases, CRT-006-2000) with application of an InGa alloy as an adhesive to ensure good thermal conductivity between the silicon substrate and the sample holder.

OLED fabrication and EL measurements

The OLED devices were fabricated by thermal evaporation under a high vacuum (ca. 7×10^{-4} Pa) onto clean ITO-coated glass substrates. Current density−voltage−luminance (*J*-*V*-*L*) characteristics were obtained using a semiconductor parameter analyzer (Agilent, E5273A) with an optical power meter (Newport, 1930C). The EL spectra of the OLEDs were obtained using a multichannel spectrometer (Ocean Optics, SD2000).

References

1. Pope, M., Kallmann, H. P. and Magnante, P. Electroluminescence in organic crystals. *J. Chem. Phys*. **38**, 2042–2043 (1963).

2. Tsutsui, T. & Saito, S. *OrganicMultilayer-Dye Electroluminescent Diodes—Is There Any Difference with Polymer LED?* (Kluwer Academic, Dordrecht, 1993).

3. Rothberg, L. J. & Lovinger, A. J. Status of and prospects for organic electroluminescence. *J. Mater. Res.* **11**, 3174–3187 (1996).

4. Wilson, J. S., Dhoot, A. S., Seeley, A. J. A. B., Khan, M. S., Köhler, A. & Friend, R. H. Spin-dependent exciton formation in π-conjugated compounds. *Nature* **413**, 828-831 (2001).

5. Segal, M., Baldo, M. A., Holmes, R. J., Forrest, S. R. & Soos, Z. G. Excitonic singlet-triplet ratios in molecular and polymeric organic materials. *Phys. Rev. B* **68**, 075211 (2003).

6. Honda, K. (ed.) *Electroluminescence in Organic Thin Films "Photochemical Processes in Organized Molecular Systems"* (Elsevier Sci. Pub., 1991).

7. Kido, J., Nagai, K. & Ohashi, Y. Electroluminescence in a terbium complex. *Chem. Lett.* 19, 657-660 (1990).

8. Baldo, M. A., Lamansky, S., Burrows, P. E., Thompson, M. E. & Forrest, S. R. Very

high-efficiency green organic light-emitting devices based on electrophosphorescence. *Appl. Phys. Lett.* **75**, 4–6 (1999).

9. Adachi, C., Baldo, M. A., Thompson, M. E. & Forrest, S. R. Nearly 100% internal phosphorescence efficiency in an organic light emitting device. *J. Appl. Phys.* **90**, 5048–5051 (2001).
10. Endo, A., Ogasawara, M., Takahashi, A., Yokoyama, D., Kato, Y. & Adachi, C. Thermally activated delayed fluorescence from Sn^{4+}–porphyrin complexes and their application to organic light-emitting diodes — A novel mechanism for electroluminescence. *Adv. Mater.* **21**, 4802–4806 (2009).
11. Endo, A., Sato, K., Yoshimura, K., Kai, Takahiro, Kawada, A., Miyazaki, H. & Adachi, C. Efficient up-conversion of triplet excitons into a siglet state and its application to organic light emitting diodes. *Appl. Phys. Lett.* **98**, 0833021–0833023 (2011).
12. Akai, N., Kudoh, S. & Nakata, M. Lowestexcited tiplet states of 1,2- and 1,4-dicyanobenzenes by low-temperature matrix-isolation infrared spectroscopy and density-functional-theory calculation. *Chem. Phys. Lett.* **371**, 655–661 (2003).
13. Wakamiya, A., Mori, K., & Yamaguchi, S. 3-Boryl-2,2’-bithiophene as a Versatile core skeleton for full-color highly emissive organic solids. *Angew. Chem. Int. Ed.* **46**,

4273–4276 (2007).

14. Adamo, C. & Barone, V. Toward reliable density functional methods without adjustable parameters: The PBE0 model. *J. Chem. Phys.* **110**, 6158–6170 (1999).

15. Hariharan, P. C. & Pople, J. A. The Influence of Polarization Functions on Molecular Orbital Hydrogenation Energies. *Theoret. Chim. Acta.* **28**, 213–222 (1973).

16. Frisch, M. J. et al. *Gaussian 09, Revision C.01,* Gaussian, Inc., Wallingford, CT, 2010.

17. Goushi, K., Yoshida, K., Sato, K. & Adachi, C. Organic light-emitting diodes employing efficient reverse intersystem crossing for triplet-to-singlet state conversion. *Nat. Photonics* **6**, 253 - 258 (2012).

18. Turro, N. J. *Modern Molecular Photochemistry* (The Benjamin/Cummings Publishing Company, Menlo Park, 1978).

Acknowledgements

This work was supported in part by the Funding Program for World-Leading Innovative R&D on Science and Technology (FIRST). H.U. sincerely thanks Grand-in-Aid for JSPS Fellows. We also thank Dr. Hajime Nakanotani, Dr. Jun-ichi Nishide and Dr. William Potscavage for their assistance for this research.

Contributions

H.U. performed the molecular design. H.U. and H.N. performed the synthetic work. K. S. performed the computational experiments. H.U. and K.G. carried out the measurements of the PL and EL characteristics. All authors co-wrote the paper. C.A. supervised the project.

Author information

Affiliations

Center for Organic Photonics and Electronics Research (OPERA), Kyushu University

744 Motooka, Nishi, Fukuoka 819-0395, Japan

Hiroki Uoyama, Kenichi Goushi, Katsuyuki Shizu, Hiroko Nomura, and Chihaya Adachi*

Competing financial interests

The authors declare no competing financial interests.

Corresponding author

Correspondence to: Chihaya Adachi

Figure captions

Figure 1: Energy diagram of conventional organic molecule and molecular structures of CDCBs.

Figure 2: Photoluminescence characteristics of 4CzIPN. (a) UV-vis absorption and photoluminescence spectra of 4CzIPN in toluene. (b) HOMO and (c) LUMO of the ground state (S_0) of 4CzIPN. (d) Electron-density difference $\Delta\rho$ between the lowest singlet excited state (S_1) and S_0 states of 4CzIPN. Blue shows where values are negative; yellow shows where values are positive. (e) Calculated differences between S_1 and S_0 state bond lengths (Å) in dicyanobenzene moiety of 4CzIPN. N_3, N_4, N_5 and N_6 atoms belong to carbazolyl groups. Atoms of the carbazolyl groups other than N_3, N_4, N_5 and N_6 atoms are not shown in Fig. 1 (e).

Figure 3: Photoluminescence (PL) of the series of CDCBs. (a) PL spectra of measured in toluene. (b) Photographs under irradiation at 365 nm.

Figure 4: Temperature dependence of photoluminescence characteristics in 6 wt% 4CzIPN:CBP film. (a) PL decay curves of 6 wt% 4CzIPN:CBP film at 300 K (black

line), 200 K (red line), and 100 K (blue line). The PL decay curves show integrated 4CzIPN emission. The excitation wavelength of the films was 337 nm. (b) The PL spectrum was resolved into prompt and delayed components. (c) Temperature dependence of PL quantum efficiencies for total (black squares), prompt (red circles), and delayed (blue triangles) components of 4CzIPN emission for 6 wt% 4CzIPN:CBP film. (d) Arrhenius plot of the reverse ISC rate from the triplet to the singlet state of 4CzIPN with k_{ISC} set to 4×10^7 (1/s).

Figure 5: Performance characteristics of the OLEDs using CDCB derivatives. External EL quantum efficiency as a function of current density for the OLEDs using CDCB derivatives as emitters. 4CzIPN (green dots), 4CzTPN-Ph (red dots), and 2CzPN (blue dots) were used as emitters. Inset: the EL spectra of the green (green line), orange (red line), and sky-blue (blue line) OLEDs at a current density of 10 mA/cm^2.

(a)

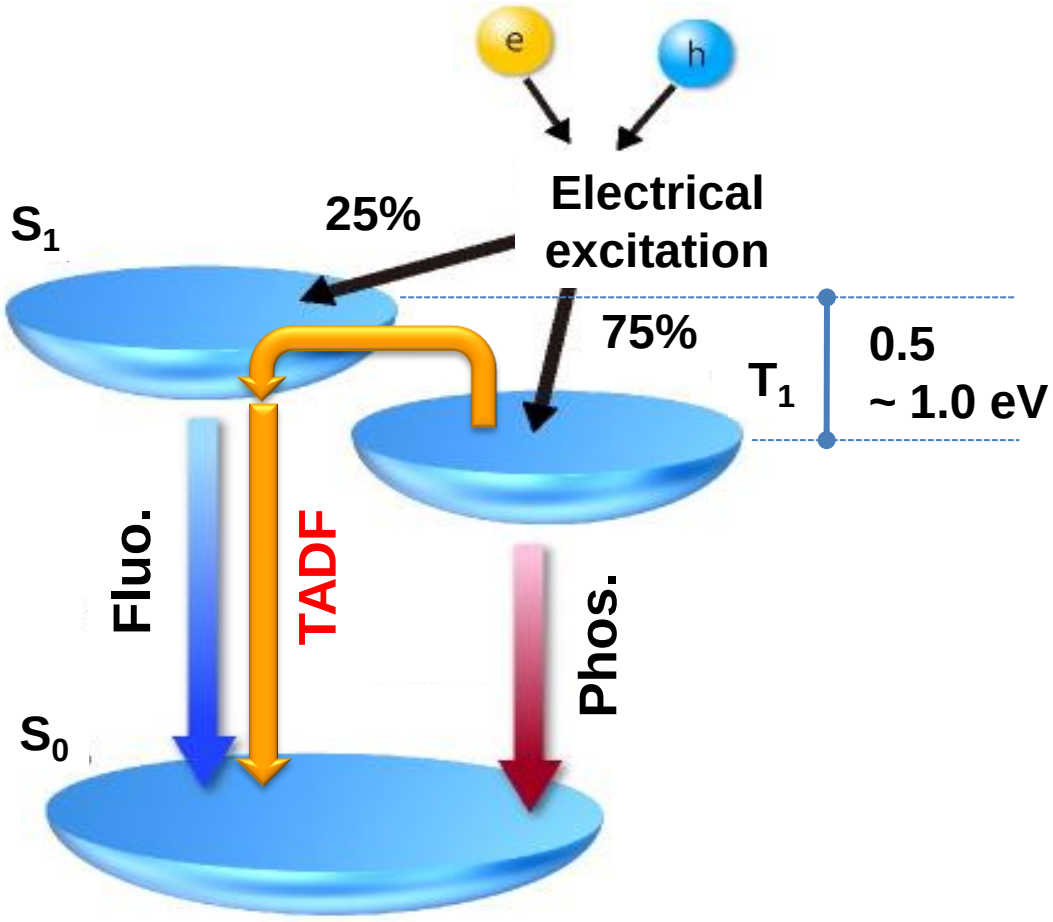

(b)

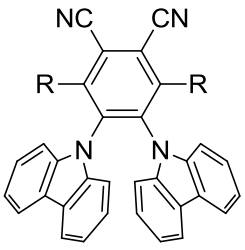

4CzPN: R = carbazolyl
2CzPN: R = H

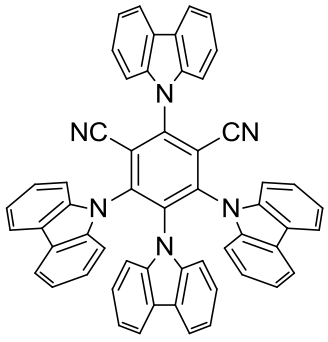

4CzIPN

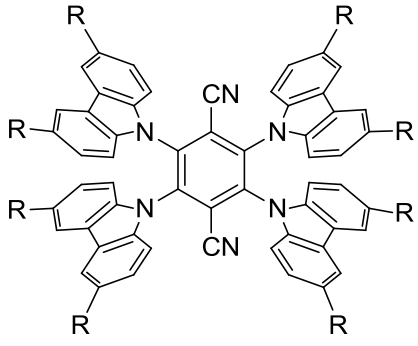

4CzTPN: R = H
4CzTPN-Me: R = Me
4CzTPN-Ph: R = Ph

Figure 1

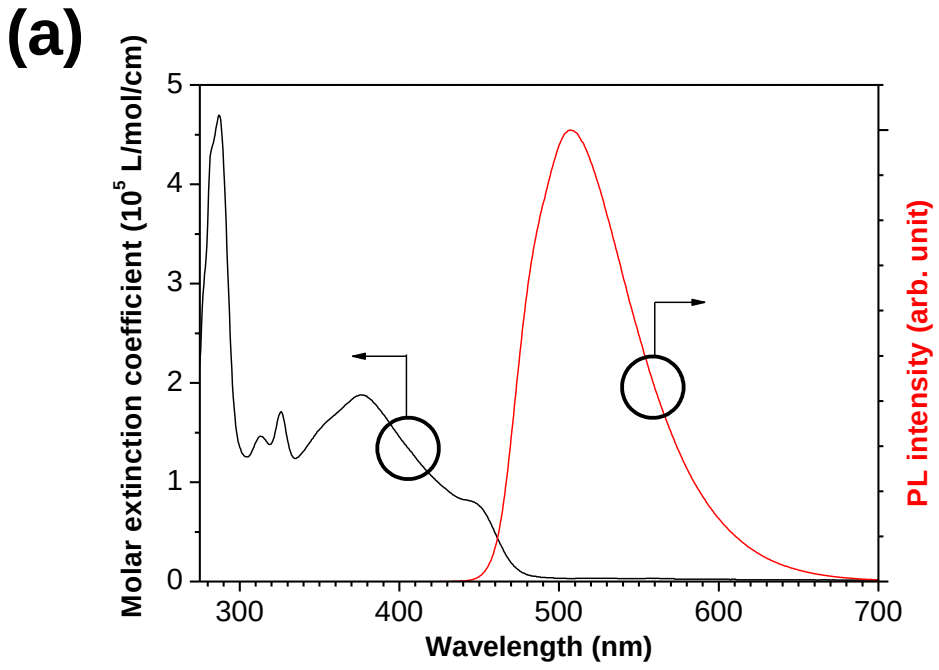
(a)
Molar extinction coefficient (10^5 L/mol/cm)
PL intensity (arb. unit)
Wavelength (nm)
0
1
2
3
4
5
300
400
500
600
700

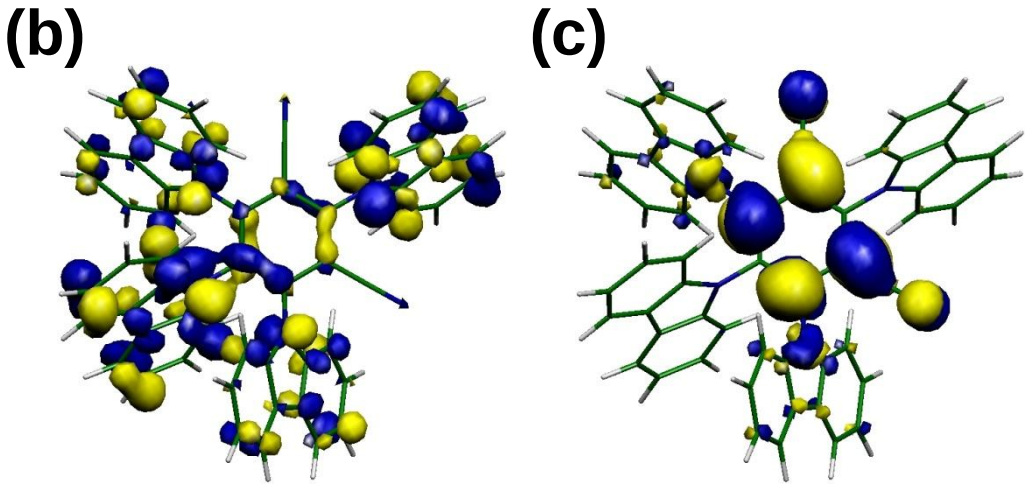
(b)
(c)

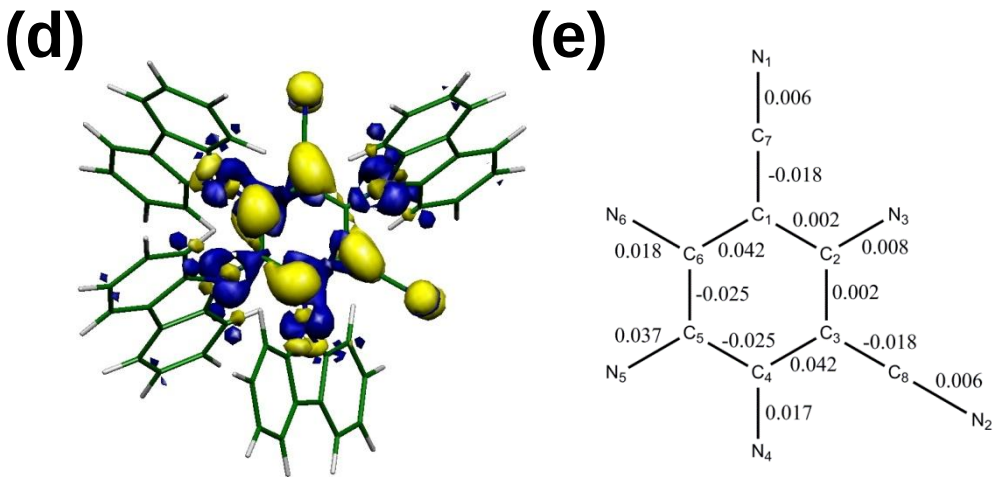
(d)
(e)
N1
0.006
C7
-0.018
N6
C1
0.002
N3
0.018
C6
0.042
C2
0.008
-0.025
0.002
0.037
C5
-0.025
C3
-0.018
N5
C4
0.042
C8
0.006
N2
0.017
N4

Figure 2

(a)

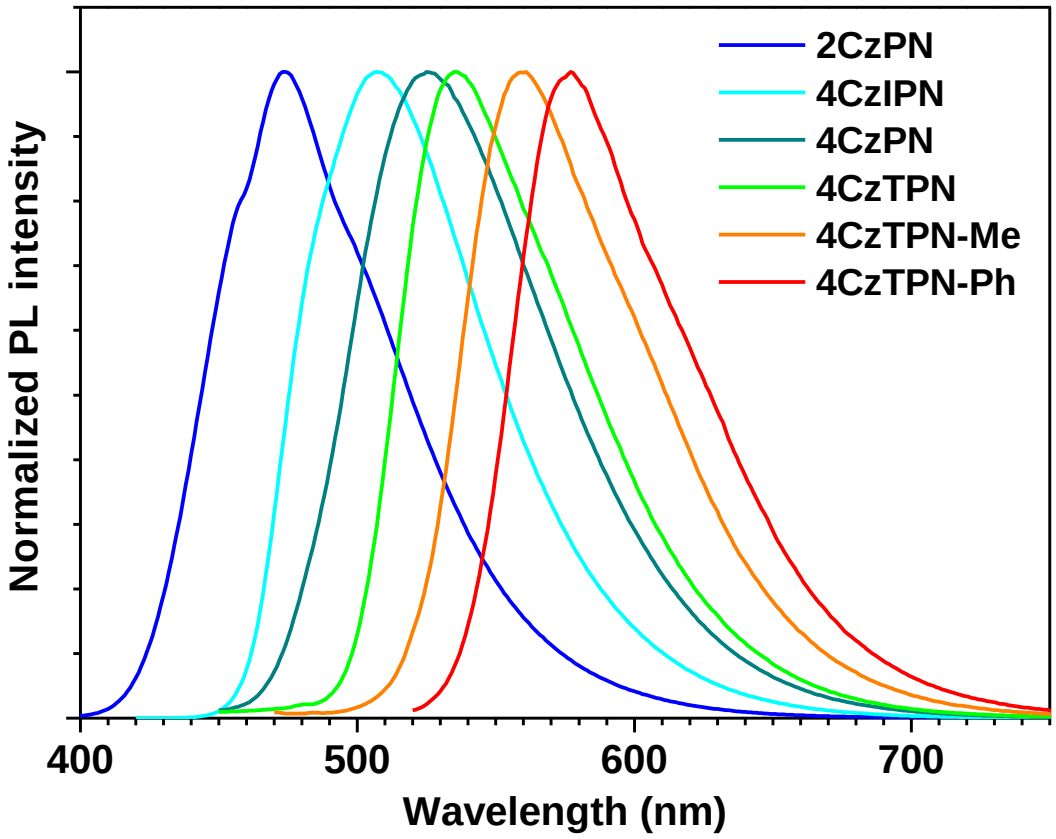
2CzPN
4CzIPN
4CzPN
4CzTPN
4CzTPN-Me
4CzTPN-Ph
Normalized PL intensity
400
500
600
700
Wavelength (nm)

(b)

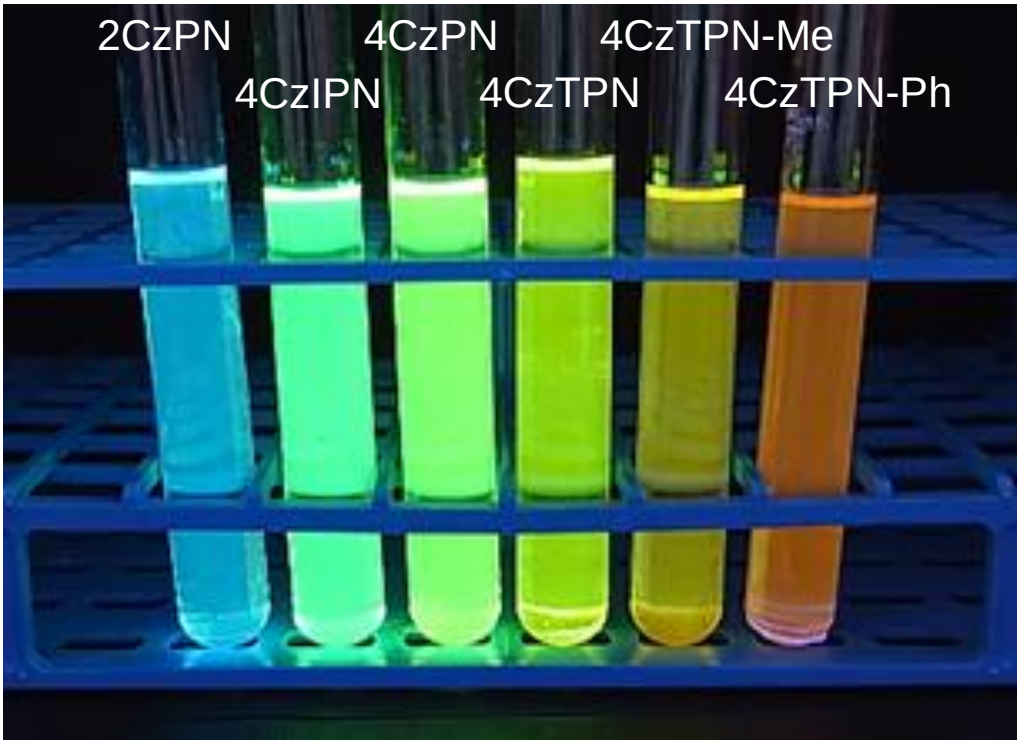
2CzPN
4CzIPN
4CzPN
4CzTPN
4CzTPN-Me
4CzTPN-Ph

Figure 3

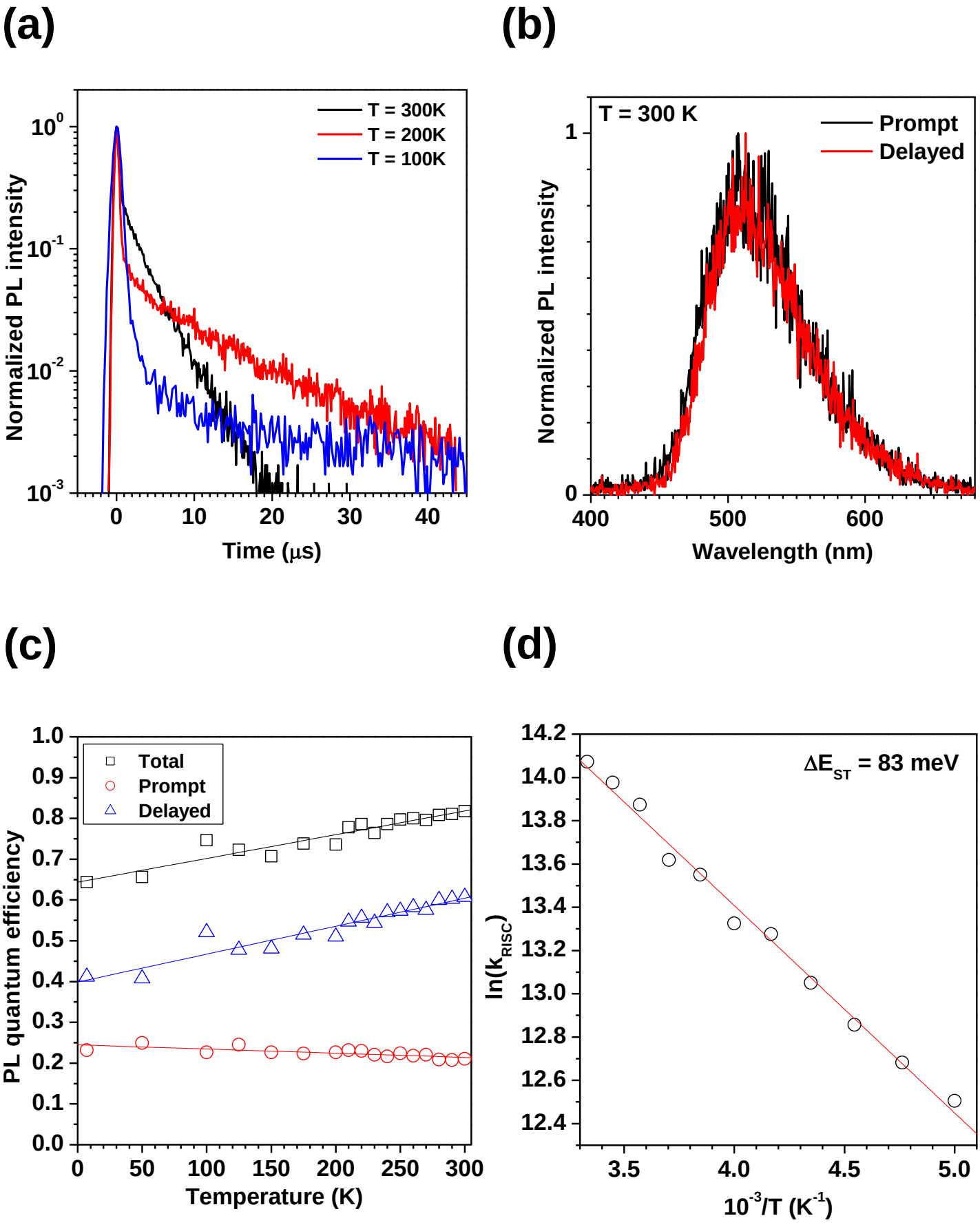
(a)
T = 300K
T = 200K
T = 100K
Normalized PL intensity
Time (μs)
(b)
T = 300 K
Prompt
Delayed
Normalized PL intensity
Wavelength (nm)
(c)
Total
Prompt
Delayed
PL quantum efficiency
Temperature (K)
(d)
ΔE_ST = 83 meV
ln(k_RISC)
10^-3/T (K^-1)

Figure 3

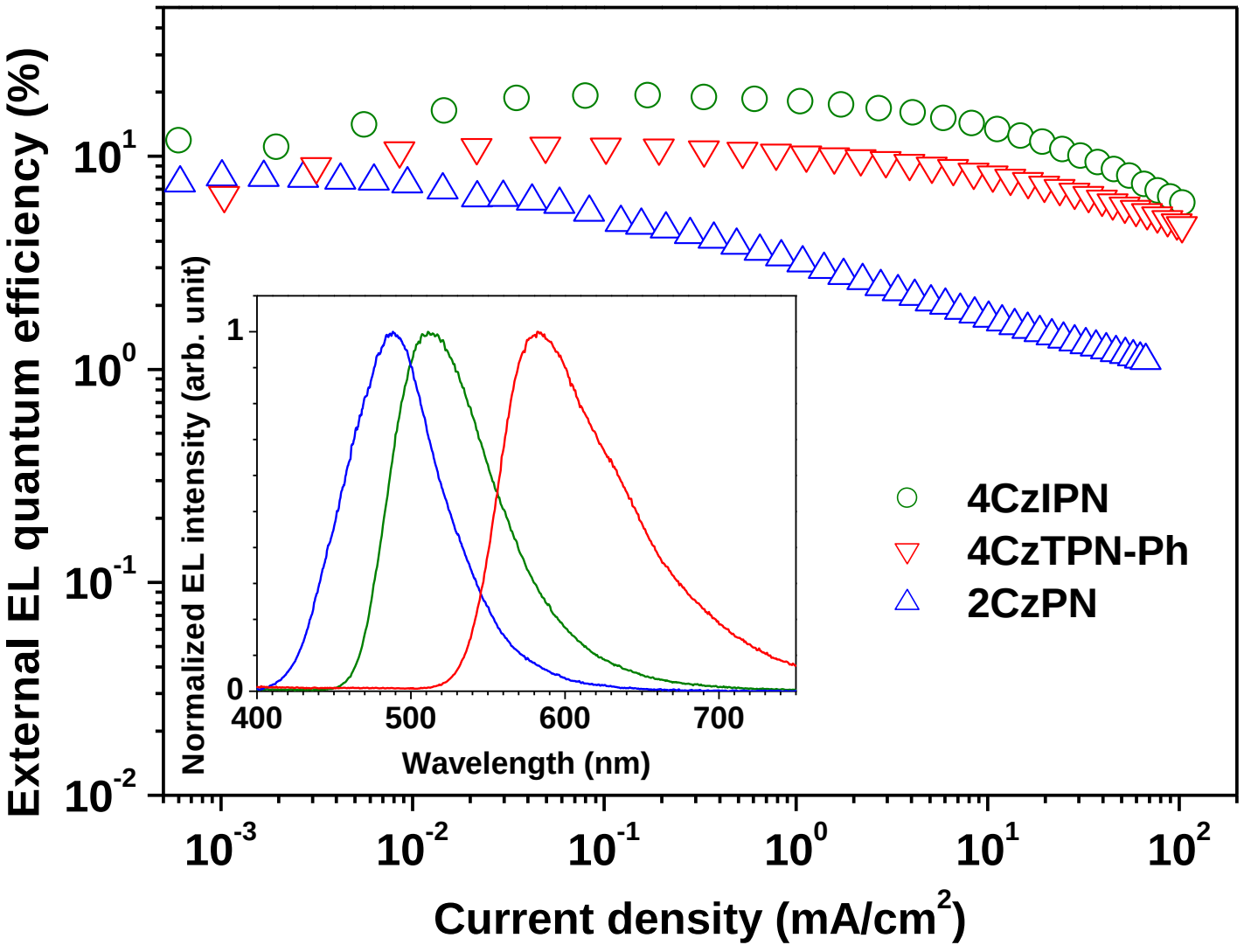
External EL quantum efficiency (%)
10^1
10^0
10^-1
10^-2
10^-3
10^-2
10^-1
10^0
10^1
10^2
Current density (mA/cm^2)
4CzIPN
4CzTPN-Ph
2CzPN
Normalized EL intensity (arb. unit)
1
0
400
500
600
700
Wavelength (nm)

Figure 5